J Solid State Electrochem (2005) 9: 476–482
DOI 10.1007/s10008-004-0580-3

ORIGINAL PAPER

C. N. Tharamani · F. Shafia Hoor
Noor Shahina Begum · S. M. Mayanna

Microstructure, surface and electrochemical studies of electroless Cr–P coatings tailored for the methanol oxidative fuel cell

Received: 17 June 2004 / Accepted: 21 July 2004 / Published online: 24 February 2005

Abstract Cr–P is a new material of great importance as a decorative coating with nickel in automobile industries. Electroless plating of Cr–P alloy has been carried out using a suitable plating bath solution and working conditions. The deposit is characterized by X-ray diffraction, transmission electron microscopy, energy-dispersive X-ray diffraction, X-ray photoelectron spectroscopy and polarization techniques. New phases appear on heat treatment of the coating. The composition (Cr/P) of the coating and the oxidation states of alloying elements vary from the surface to the bulk of the material. The coatings acted as a novel electrode material with good electrocatalytic activity (low overvoltage) and good corrosion resistance for anodic oxidation of methanol in H_2SO_4 at normal working temperature. The good corrosion resistance of the Cr–P film is accounted for by the existence of a double oxyhydroxide passive film on the surface. The electrocatalytic activity of Cr–P is very high when compared with chromium alone.

Keywords Electroless plating · Cr–P coating · Methanol oxidation · Overvoltage · Corrosion resistance

Introduction

Chromium is a versatile metal because it retains tarnish, corrosion, wear and scratch resistance even under severe service conditions [1]. Electroplated chromium coatings find widespread applications in metal finishing industries, especially in automobile industries. However, the process of development has several drawbacks [2] from environmental and economical points of view. Phosphorous is a metalloid, addition of which to chromium in traces may impart better corrosion resistance [3]. In recent years, electroless plating has been gaining importance over electroplating in producing surface coatings [4]. In this direction, a few attempts have been made in our laboratory to produce Fe–P, Ni–P, Fe–P–Pt, Fe–P–Mo and Fe–P–W coatings as new materials for functional application [5, 6, 7]. Electroless plating bath solutions and working conditions have been developed to get good quality Cr–P alloys for corrosion resistance applications [8].

The methanol oxidative fuel cell is a promising power source in electrically driven vehicles [9]. The technological development of the system has been very slow because of the use of high-priced platinum group metals as electrodes and electrode surface inhibition by the oxidation reaction intermediates [10]. Extensive literature is available on this subject and the use of platinum composites with Ru and WO_3 and Ni–Pd alloys is noteworthy [11, 12, 13]. However, the preparative procedures of the previously mentioned materials are tedious and economically viable.

The present communication reports some preliminary results on the characterization of electroless coating of Cr–P alloys as electrocatalysts for anodic oxidation of methanol in H_2SO_4. Attempts are made to account for the electrocatalytic activity of the coating on the basis of the results obtained from the microstructural and surface analyses by X-ray diffraction (XRD) and X-ray photoelectron spectroscopy (XPS) studies, respectively. The coatings proved to be promising stable anode materials in fuel cell electrolytes. The method of preparation of the electrode material is simple and economical.

Experimental

All solutions were prepared by using analytical reagent grade chemicals and double-distilled water. Alloys of

C. N. Tharamani · F. Shafia Hoor · N. Shahina Begum
S. M. Mayanna (✉)
Department of Post-Graduate Studies and Research in Chemistry,
Central College Campus, Bangalore University,
560 001 Bangalore, India
E-mail: smm_chem@yahoo.co.in
Tel.: +91-80-23301726
Fax: +91-80-2321929

Cr–P were coated on copper foils (99% pure, 10 mm×10 mm×0.25 mm) using a suitable bath solution. Prior to deposition, copper foils were precleaned using the procedures described elsewhere [14]. Surface activation was done for 5 s in $SnCl_2$ solution (0.2 g $SnCl_2$ in 1 ml HCl diluted to 100 ml with water) followed by $PdCl_2$ solution (0.1 g $PdCl_2$ in 1 ml HCl diluted to 100 ml with water) before deposition [15]. The ratio of the volume of the solution to the area of the substrate was maintained at 30 ml/cm^2. Polarization on prepared alloy samples was carried out in a CH_3OH and H_2SO_4 mixture under galvanostatic conditions using a potentiostat/galvanostat (EG&G PAR 362). A large platinum foil and a saturated calomel electrode were used as auxiliary and reference electrodes, respectively. A fine drawn capillary was used to minimize *IR* drop.

XRD patterns of the deposited films were obtained with a Philips PW 1140/90 diffractometer using Cu Kα radiation and a Ni filter. Transmission electron microscopy of the film was carried out in a JEOL 200-CX transmission electron microscope operated at 200 kV. Alloys were destripped in dilute HNO_3 solution, and the Cr and P contents in the alloys were obtained spectrophotometrically using 1,5-diphenyl carbazide [16] and acid molybdate [17] as reagents, respectively. A few samples were subjected to heat treatment (623 K) for 5 h under a N_2 atmosphere.

X-ray photoelectron spectra of the deposited alloys were recorded using a ESCA-III mark 2 spectrometer (VG Scientific, UK) using Al Kα radiation with a photon energy of 1,486.6 eV. The binding energies were calculated with respect to the C(1*s*) peak at 285 eV with a precision of ±0.2 eV. For XPS analysis, the samples were placed into an ultrahigh vacuum chamber at 10^{-9} Torr housing the analyser. Prior to mounting, the samples were kept in the preparation chamber at ultrahigh vacuum for 5 h in order to desorb any volatile species present on the surface. Intermittent sputtering was performed by using a defocused Ar^+ ion beam at low voltage and current over an area of 0.8×2.4 mm^2.

Sputtering was carried out to remove successive layers of a few angstroms and material in a particular layer. The experimental data were curve-fitted with Gaussian peaks after subtracting a linear background. For Gaussian peaks, a slightly different full width at half maximum (FWHM) was used for different chemical states. The spin–orbit splitting and the doublet intensities were fixed as given in the literature [18]. The concentrations of different chemical states were evaluated from the area of the respective Gaussian peaks.

Results and discussion

Electroless deposition of Cr–P alloy

Complexing agents play a significant role in the plating bath solution in producing good-quality coatings [19]. Hence, attempts were made to select a suitable complexing agent for Cr^{3+} ions. Detailed spectrophotometric analysis of Cr^{3+} ions with several complexing agents at pH 3.0 revealed that only potassium thiocyanate (KSCN) affords a suitable complex with Cr^{3+} ions. O the basis of the preliminary plating experiments, the following bath composition and plating conditions were fixed to get a good-quality Cr–P alloy.

Bath composition: 0.1 M $Cr_2(SO_4)_3{\cdot}6H_2O$ as a source of Cr^{3+} ions and 0.1 M NaH_2PO_2 H_2O as a reducing agent which reduces Cr^{3+} ions to Cr during plating. KSCN (0.1–0.2 M) was used as a complexing agent for Cr^{3+} ions, and 20 g/l H_3BO_3 and 10 g/l NaCl were used as a buffering agent and a conduction salt, respectively, and in combination they suppress the rate of codeposition of H_2 gas [20]. $NaNO_2$ was employed as a reducing agent to convert Cr^{6+} ions (if any) to Cr^{3+} ions.

Plating conditions: pH 3.0, temperature 323 K, substrate copper foil, Time 1–3 h.

The coatings prepared under different experimental conditions were used for microstructure, surface and electrocatalytic analysis.

Microstructure and surface characterization

The coating obtained under fixed experimental conditions was subjected to energy-dispersive X-ray diffraction analysis which confirmed the presence of both Cr and P in the coating (Fig. 1). The XRD patterns of the deposited Cr–P alloy indicated the crystalline nature and also the existence of new phases in the heat-treated sample (Table 1). The grain size of the coating was evaluated (198 Å) from the XRD pattern using Debye–Scherrer equation [21] (FWHM). The ring-type diffraction pattern of the Cr–P coating is shown in Fig. 2, and

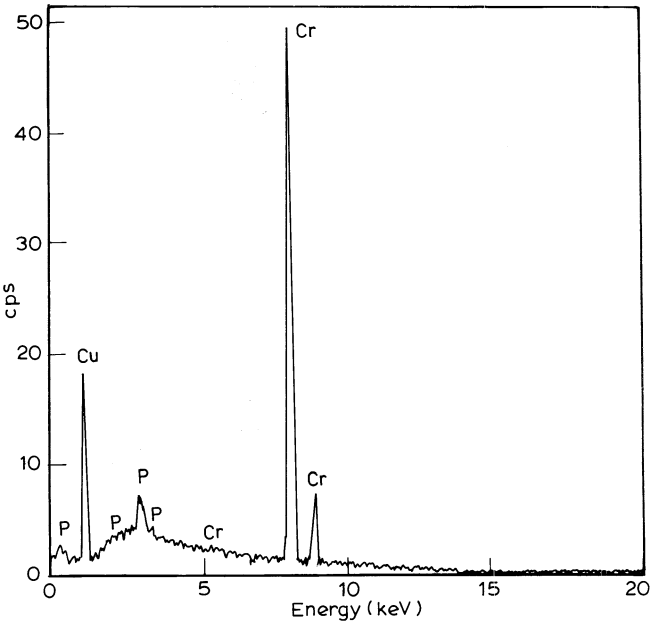

Fig. 1 Energy dispersive X-ray analysis of Cr–P alloy (as prepared)

Table 1 X-ray diffraction data of Cr–P alloy

As deposited			After heat-treatment[a]		
Observed d (Å)	Std. ASTM d (Å)[b]	Phase	Observed d (Å)	Std. ASTM d (Å)[b]	Phase
2.46	2.46	CrP(111)	2.19	2.19	$Cr_{12}P_7$(211)
2.15	2.16	Cr_3P(112)	1.87	1.87	Cr_3P(222)
1.88	1.87	CrP(103)	1.27	1.25	Cr_3P(413)
1.83	1.81	P(121)	1.20	1.20	P(206)
1.27	1.25	Cr_3P(413)			

[a]623 K under N_2 atmosphere for 5 h
[b]1999 JCPDS-International Centre for Diffraction Data, PCPDFWIN v. 1.30. Target, Cu Kα; filter, Ni

could be indexed as Cr–P alloy agreeing well with the XRD results [22].

XPS spectra of Cr(2*p*) core-level regions of the plated Cr–P sample are shown in Fig. 3. It is evident from the figure that the binding energy of the Cr $2p_{3/2}$ core level is higher and it decreases on heat treatment at 673 K. The shift in the binding energy after heat treatment suggests a change in the chemical state of Cr. The Cr($2p_{3/2,1/2}$) peaks at 576.8 and 586.0 eV are attributed to Cr^{3+} in the surface film. However, after 10- and 20-min sputtering these peaks appeared at 573.3 and 584.7 eV (Table 2), indicating the metallic state Cr^0.

The XPS spectrum of the P(2*p*) region of the deposited film shows a peak at 133.2 eV (Fig. 4a) which could be assigned to the P^{5+} species since the P(2*p*) peak in Na_2HPO_4 occurs at 133.1 eV [23]. It is seen from the spectrum that P(2*p*) peaks occur at 129.6 and 133.0 eV after 10- and 20-min sputtering (Fig. 4b, c), respectively. The higher binding energy peak can be attributed to P^{5+} species only. The binding energy for the P(2*p*) level in red phosphorous is 130.2 eV [23]; therefore, the P(2*p*) peak is shifted by −0.6 eV with respect to the P(2*p*) peak of red phosphorus. The direction of shift of the 2*p* emission of P shows that it is in a negatively charged state ($P^{\delta-}$). XPS spectra of P(2*s*) core-level regions of the deposited sample without and with sputtering are shown in Fig. 5. The binding energy of P(2*s*) in phosphorous is 189.0 eV. The observed P(2*s*) peak at 191.0 eV (Fig. 5a) indicates the presence of P^{5+} species in the sample. The XPS spectra of the P(2*s*) core-level region after 10- and 20-min sputtering show two peaks at 187.5 and 191.1 eV (Fig. 5b, c) indicating the presence of $P^{\delta-}$ as well as P^{5+} species in the sputtered sample. The binding energies and the relative intensities of P(2*p*) and P(2*s*) core levels with different P species are given in Table 2. The heat

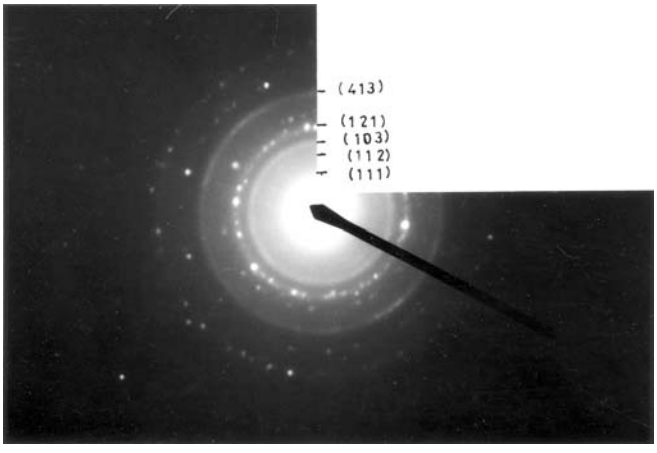

Fig. 2 Ring-type electron diffraction pattern of as-prepared Cr–P alloy

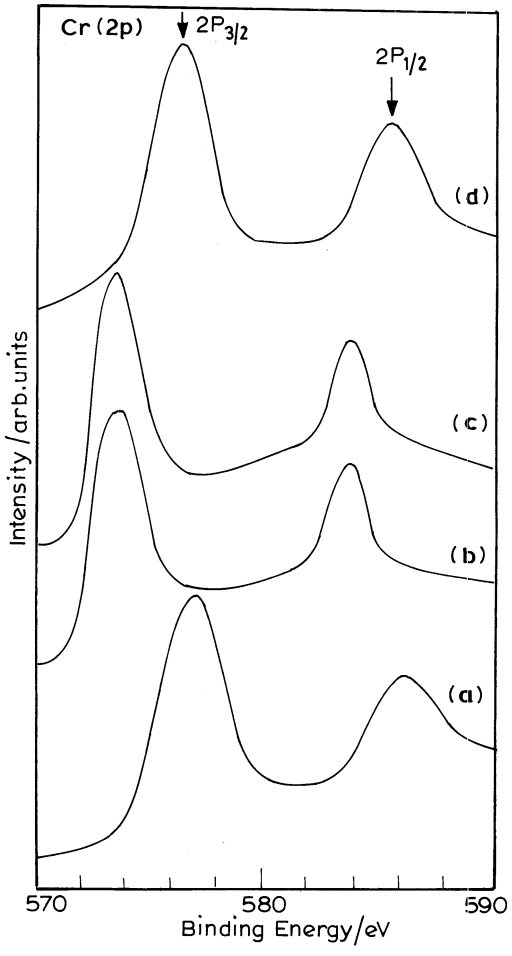

Fig. 3 X-ray photoelectron spectrum (*XPS*) of the Cr(2*p*) core-level region of Cr–P alloy film: as prepared (*a*), after 10-min sputtering (*b*), after 20-min sputtering (*c*), after heat-treatment (*d*)

Table 2 Binding energies of different Cr, P and O species under different conditions. Values for O^{2-}, OH^- and H_2O species after 10-min sputtering are given in *parentheses*

Chemical state	Binding energy (eV)
Cr(2$p_{3/2}$)	
Cr^{3+}	576.8
Cr^{0a}	573.3
Cr(2$p_{1/2}$)	
Cr^{3+}	586.0
Cr^{0a}	584.7
P(2p)	
P^{5+}	133.2
P^{5+a}	133.0
$P^{\delta-a}$	129.6
P(2s)	
P^{5+}	191.0
P^{5+a}	191.1
$P^{\delta-a}$	187.5
O(1s)	
O^{2-}	530.0 (530.2)
OH^-	531.7 (532.0)
H_2O	533.7 (533.5)

[a]After 10-min sputtering

treated film shows two peaks at 129.5 and 133.3 eV in the P(2p) region indicating the presence of both $P^{\delta-}$ and P^{5+} species in the film.

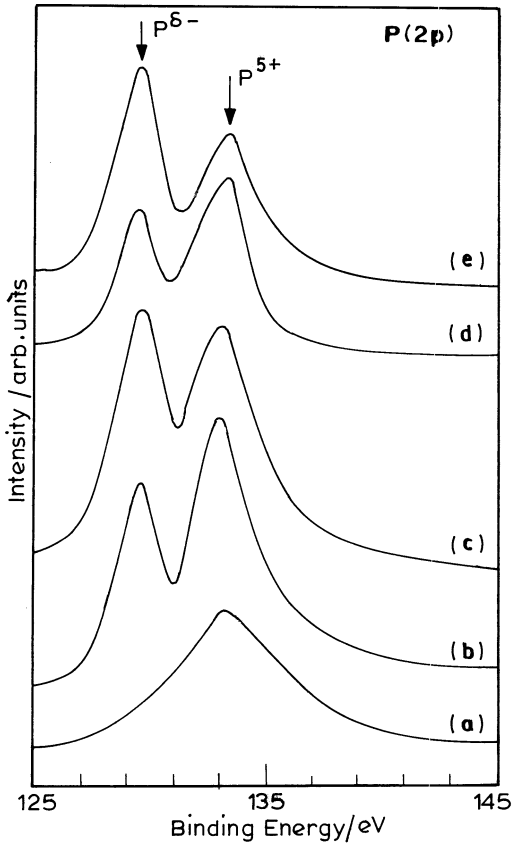

Fig. 4 XPS of P(2p) core-level regions of Cr–P alloy film: as prepared (*a*), after 10-min sputtering (*b*), after 20-min sputtering (*c*), after heat treatment (*d*), after heat-treatment and 10-min sputtering (*e*)

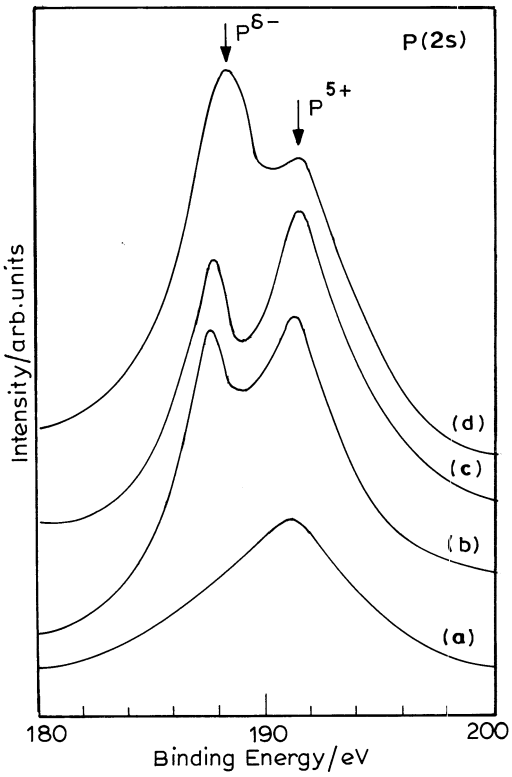

Fig. 5 XPS of the P(2s) core-level region of Cr–P alloy film: as prepared (*a*), after 10-min sputtering (*b*), after 20-min sputtering (*c*), after heat-treatment (*d*)

Figure 6 presents the XPS spectrum of the oxygen 1s core-level regions for the deposited samples without and with 10- and 20-min sputtering. The spectrum of the O(1s) electron binding energy region consists of three peaks originating from O^{2-}, hydroxide or a hydroxyl group (OH^-) and hydrate and/or adsorbed water. The O(1s) spectrum shows an intense peak at 531.7 eV along with a weak peak at 530.0 eV. The lower binding energy peak could be attributed to O^{2-} species associated with oxides of chromium, whereas the higher binding energy

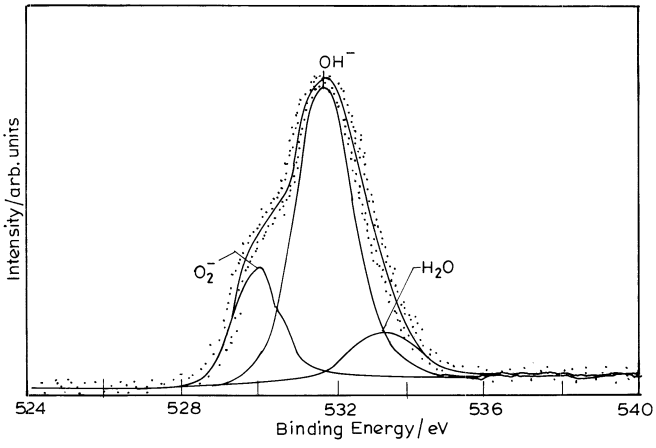

Fig. 6 XPS of O(1s) core-level regions of Cr–P alloy film

peak is responsible for P^{5+} species [23]. A comparison of the relative intensities of the two O(1*s*) peaks shows that the amount of oxygen associated with P is more than that associated with Cr. Taking this fact into consideration along with the observation that the deposited film contains P^{5+}, we expect that the most probable species for the higher binding energy O(1*s*) peak could be due to phosphate (PO_4^{3-}). The intensity of the peak at 531.7 eV decreases after 10- and 20-min sputtering. These observations infer that O^{2-} type species predominate in the sputtered film compared with oxygen associated with phosphorous, suggesting the reduction of PO_4^{3-} to $P^{\delta-}$. A weak peak at 533.7 eV indicates the presence of a H_2O component in the sample, which decreases on sputtering. The binding energies and relative intensities of O(1*s*) peaks in the deposited sample and after 10- and 20-min sputtering are given in Table 2.

The binding energy at 576.8 eV in the deposited film belongs to that of Cr in the hydroxide [$Cr(OH)_3$ or CrOOH] form. Similarly, the binding energy of 576.3 eV for the Cr $2p_{3/2}$ core level in the heat-treated sample corresponds to that of Cr in the oxide Cr_2O_3 [24]. It was reported in earlier studies that after heat-treatment the sample undergoes transition from hydroxides to oxides. The change in chemical state of Cr from hydroxide to oxide leads to the loss of oxygen and hydrogen (in the form of water molecules). These results show that the film consists of mixed oxyhydroxides of Cr, which passivate the surface and improve and the corrosion resistance of the Cr–P alloy.

The surface concentration ratio of Cr(2*p*) to P(2*p*) can be evaluated by the relation

$$\frac{C_{\mathrm{Cr}}}{C_{\mathrm{P}}} = \frac{I_{\mathrm{Cr}}\sigma_{\mathrm{P}}\lambda_{\mathrm{P}}D_{\mathrm{E}}(\mathrm{P})}{I_{\mathrm{P}}\sigma_{\mathrm{Cr}}\lambda_{\mathrm{Cr}}D_{\mathrm{E}}(\mathrm{Cr})},$$

where C, I, σ, λ and D_{E} are the concentration, intensity, photoionization cross-section, mean escape depth and geometric factor, respectively. Integrated intensities of Cr(2*p*) and P(2*p*) peaks are accounted for by calculating the concentrations. Photoionization cross-sections and mean escape depths are taken from the literature [25, 26]. The surface concentration ratios of Cr to P in Cr–P alloy film obtained under different conditions are given in Table 3. The surface concentration ratio of Cr to P is 4.58 in the deposited film, suggesting the enrichment of Cr on the surface; however, this ratio decreased on successive sputtering. A similar trend is observed in case of the heat-treated sample.

From XPS studies it is clear that the deposited as well as the heat-treated film contains Cr^{3+} species. The decrease in intensity of the Cr^{3+} species and the appearance of metallic Cr on successive sputtering indicated that the deposit is prone to surface oxidation to some extent. Phosphorous is in P^{5+} and $P^{\delta-}$ states in the heat-treated film and the drastic increase in the concentration of $P^{\delta-}$species compared with P^{5+} species upon successive sputtering indicated the variation in the concentration of different kinds of intermetallic compounds like Cr_3P, CrP and $Cr_{12}P_7$ in the corresponding layer.

Table 3 Surface concentration ratios of Cr(2*p*) to P(2*p*) in as-prepared Cr–P alloy film at different conditions

Sample	$C_{\mathrm{Cr}}/C_{\mathrm{P}}$
As prepared	4.58
After 10-min sputtering	2.38
After 20-min sputtering	1.24

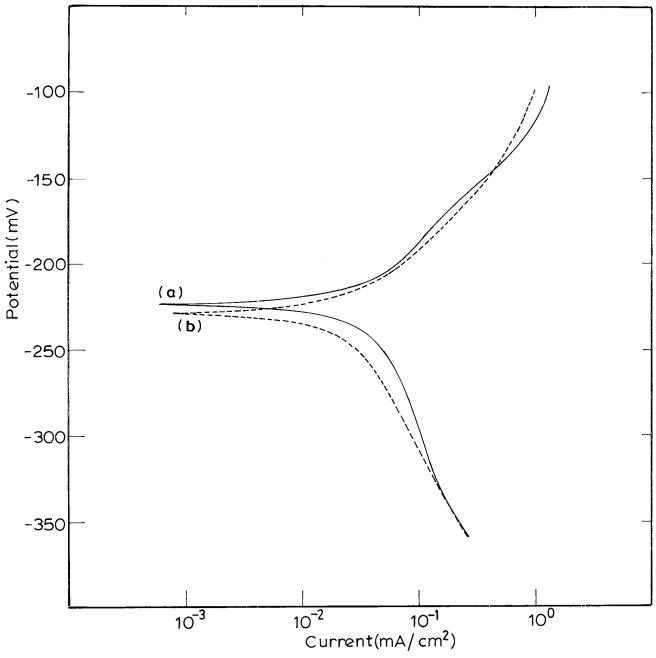

Fig. 7 Galvanostatic polarization diagrams for methanol (1 M) oxidation in H_2SO_4 (0.5 M) on Cr–P alloy as prepared (*a*, *full lines*) and after heat-treatment (*b*, *dashed lines*)

Electrochemical catalytic efficiency

H_2SO_4 is one of the electrolytes used in the methanol oxidative fuel cell [27]. In order to know whether the deposited Cr–P alloys act as an effective anode for anodic oxidation of methanol, galvanostatic polarization experiments were conducted in different concentrations of H_2SO_4 containing 1 M CH_3OH using Cr–P alloys in the current density range 1–100 mA/cm^2 at 303 K (Fig. 7). The electrochemical parameters for methanol oxidation on Cr–P alloy are given in Table 4 and indicate the improvement of catalytic activity (lowering of η) with a decrease in H_2SO_4 concentration or an increase in the concentration of methanol. Heat-treated Cr–P alloy is associated with low overpotential (η) at normal working temperature, which is much lower than the value obtained with other electrode material [28] in a similar system.

The alloys also exhibited better corrosion resistance (Table 4) in H_2SO_4. The heat-treatment of the coating further improved the corrosion resistance, as evident from the prolonged electrolysis (up to 100 h) that was

Table 4 Electrochemical parameters of Cr–P alloy during methanol oxidation (1 M CH_3OH) in 0.5 M H_2SO_4. The values for the heat-treated samples (5 h, N_2 atmosphere at 623 K) are given in *parentheses*

Cell electrolyte	b_a (mV/dec) ±5 mV vs SCE	i_{corr} ($\mu A/cm^2$)	η_{100} (mV) ±5 mV vs SCE
1 M CH_3OH + 0.5 M H_2SO_4	15.06 (13.71)	2.3 (0.72)	225 (206)
1 M CH_3OH + 0.25 M H_2SO_4	16.86 (12.85)	5.9 (1.4)	217 (200)
0.5 M CH_3OH + 0.5 M H_2SO_4	27.70 (22.98)	28.2 (18.47)	382 (339)

conducted in 0.5 M H_2SO_4 containing 1 M methanol at 303 K and current density of 100 mA/cm^2. The anode was stable and exhibited steady overpotential (±10 mV) (Fig. 8), which is one of the key characteristics of a high performing anode in a fuel cell.

The increase in catalytic activity upon heat-treatment in the present system may be attributed to the change in the nature of the surface of the deposit [29]. It is difficult to account for the electrocatalytic activity of the electrode material because it is related to several complex parameters associated with surface and bulk properties of the coating and the type of surface reaction: surface area, grain size and grain orientation, crystal structure, nature of chemical species and their composition, electronic conductivity, etc. In order to evaluate the relative increase in the surface area of C–P by alloying Cr with P, cyclic voltammetric experiments were carried out on Cr–P alloy and also on pure Cr in the potential range from −1,200 to +1,200 mV at a scan rate of 50 mV/s in a mixture of 1 M CH_3OH and 0.5 M H_2SO_4. The anodic peak current characteristic for the oxidation reaction rate on Cr–P was abnormally high (5,000 μA) compared with that for pure chromium (10 μA). On the basis of these data, the relative increase in surface area ($I_{p\ (Cr-P)}/I_{p\ (Cr)}$) by alloying the Cr with P was found to be 500 (Fig. 9). The increase in catalytic activity could be attributed to a decrease in crystal size (increase in surface area) or an increase in electronic conductivity or a change in surface characteristics, which favour oxidation of methanol on the electrode surface.

The electrooxidation of methanol is a complex process which is retarded by the adsorption of reaction intermediates like CO and formaldehyde on the electrode surface [30]. In order to identify the reaction intermediate during oxidation, cyclic voltammetric experiments were conducted. In aqueous solution under slightly acidic conditions, zinc sulphate in presence of formaldehyde gives a characteristic cyclic voltammogram [31]. In the present system, the cyclic voltammogram was obtained on a Cr–P alloy microelectrode using oxidized acidic (0.5 M H_2SO_4) methanol solution containing zinc sulphate. These results are compared with those obtained in acidic zinc sulphate solution containing formaldehyde. Identical results (Fig. 10) were obtained and confirm the presence of formaldehyde as an intermediate during the oxidation of methanol in H_2SO_4. A small portion of oxidized solution was coloured with chromotropic acid and the UV absorption spectrum was taken. The absorption at 570 nm further confirms the presence of formaldehyde as a reaction intermediate [30].

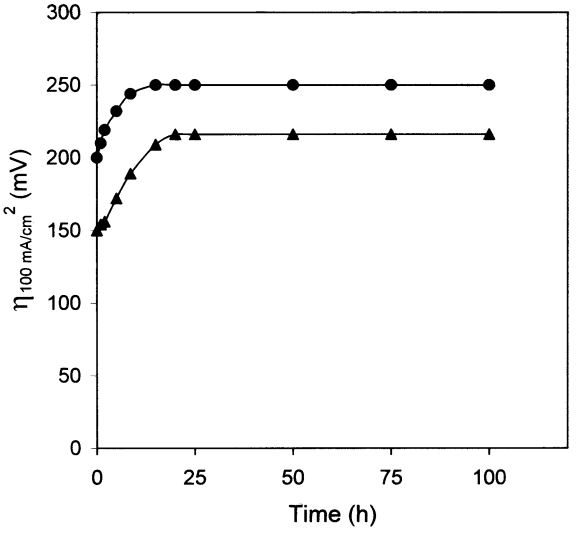

Fig. 8 Variation of over potential (η at 100 mA/cm^2) with time on coated alloys in 1 M CH_3OH and 0.5 M H_2SO_4 under different conditions. As prepared (*circles*), after heat-treatment (*triangles*)

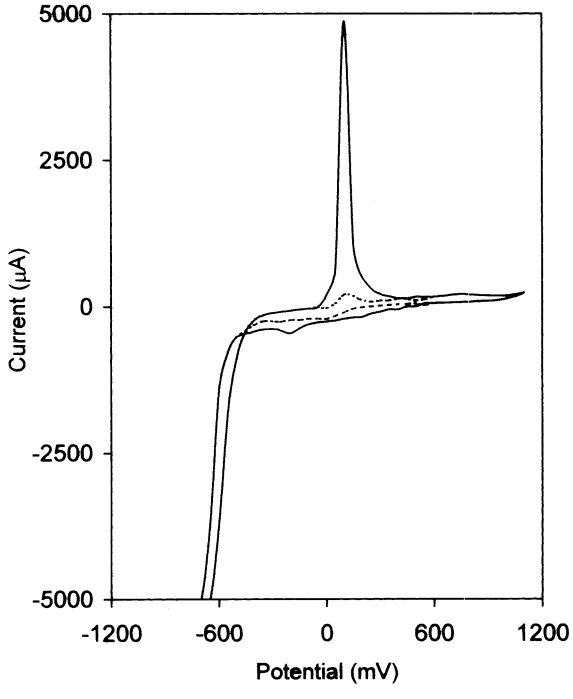

Fig. 9 Cyclic voltammograms obtained in 0.5 M H_2SO_4 and 1 M CH_3OH at a scan rate of 50 mV/s and 303 K. Cr–P alloy (*full lines*), Cr (*dashed lines*)

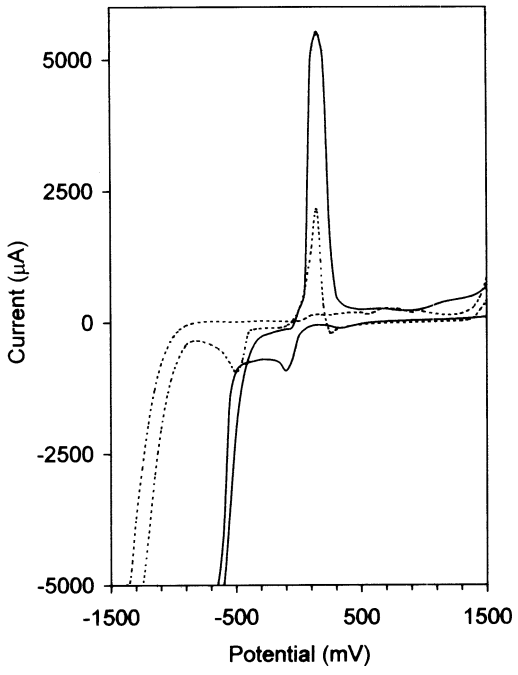

Fig. 10 Cyclic voltammograms obtained on Cr–P alloy at a scan rate of 25 mV/s and 303 K. $ZnSO_4$, Na_2SO_4 and formaldehyde (*dashed lines*), oxidized mixture of methanol in H_2SO_4 (*full lines*)

Conclusions

A plating bath and the working conditions were optimized to get a good-quality Cr–P alloy film. The oxidation states of Cr and P vary from the surface to the bulk of the coating. The surface area of Cr is enhanced by alloying it with P. The deposited alloy has tailor-made characteristics to make it a better anode material with low overvoltage for the methanol oxidative fuel cell in H_2SO_4 at normal working temperature. Heat-treatment of the deposit resulted in the formation of new phases. A cyclic voltammetric study showed the existence of formaldehyde as one of the reaction intermediates which does not interfere during oxidation of methanol.

Acknowledgements S.M.M. expresses his gratitude to the AICTE, New Delhi, for financial assistance in the form of an Emeritus fellowship.

References

1. Gabe DR (1998) Metal finishing guide book. Elsevier, New York
2. Dennis JK, Such TE (1972) Nickel and chromium plating. Butterworths, London, p 186
3. Watanabe T, Sakurai Y, Hamakaw Y, Masumoto T, Shirae K, Suzuki K (eds) (1993) Current topics in amorphous materials-physics and technology. Elsevier, New York, p 137
4. Mallory GO, Hajdu JB (eds) (1990) Electroless plating: fundamentals and applications. AESF, Orlando, FL, p 207
5. Shafia Hoor F, Aravinda CL, Ahmed MF, Mayanna SM (2000) J Mater Sci Lett 19:1067
6. Mimani T, Mayanna SM (1996) Surf Coat Technol 79:246
7. Ramesh L, Sheshadri BS, Mayanna SM (1998) Procedings of the European workshop on chemistry, energy and environment held at Lisbon, Portugal, July 1997. Royal Society special publication on chemistry, energy and environment 217:505
8. Tharamani CN, Shahina Begum N, Mayanna SM (2004) Mater Chem Phys 83:278
9. Kordesch K, Simader G (1996) Fuel cells and their applications. VCH, Weinheim, p 251
10. Matsui H (1987) Bull Chem Soc Jpn 60:863
11. Watanabe M, Uchida M, Motoo S (1987) J Electroanal Chem 229:395
12. Shen PK, Tseung ACC (1994) J Electrochem Soc 141:3082
13. Shobha T, Aravinda CL, Parthasarathi B, Gomathi Devi L Mayanna SM (2003) Mater Chem Phys 80:656
14. Mayanna SM, Setty TAV (1972) Indian J Chem 10:295
15. Mimani T, Mayanna SM (1993) Plating Surf Finish 80:66
16. Bassett J, Denney RC, Jeffery GH, Medham J (eds) (1978) Vogel's text book of quantitative inorganic analysis, 4th edn. ELBS & Longman, London, p 738
17. Merz M (1959) Microchim Acta 1959:454
18. Briggs D, Seah MP (1984) Practical surface analysis by Auger and X-ray photoelectron spectroscopy, Wiley, New York, p 503
19. Levy DJ (1963) AES Tech Proc 29
20. Mimani T, Mayanna SM (1993) J Appl Electrochem 23:339
21. Klug HP, Alexander L (eds) (1980) X-ray diffraction procedures for polycrystalline and amorphous material. Wiley, New York
22. Grundy PJ, Jones GA (1976) The structure and properties of solids 7: Electron microscopy in the study of material. Crane Russak, New York, p 19
23. Rajam KS, Rajagopalan SR, Hegde MS, Viswanathan B (1991) Mater Chem Phys 27:141
24. Asami K, Hasimoto K (1977) Corros Sci 17:559
25. Scofield J H (1976) J Electron Spectrosc Relat Phenom 8:129
26. Penn DR (1976) J Electron Spectrosc Relat Phenom 9:29
27. Hamnett A, Stevens P, Troughton GI (1990) Catal Today 7:219
28. Chunzhi He, Kunz H R, Fenton JM (1997) J Electrochem Soc 144:970
29. Adman U, Dariel MP, Grunbaun E, Lodder JC (1987) J Appl Phys 62:1943
30. Matsui H, Kunugi A J (1990) Electroanal Chem 292:103
31. Shabana Begum S, Murulidharan VS, Mayanna SM (2001) Port Electrochim Acta 19:121